

New Centre/Surround Retinex-like Method for Low-Count Image Reconstruction

V. E. Antsiperov^a

Kotelnikov Institute of Radioengineering and Electronics of RAS, Mokhovaya 11-7, Moscow, Russian Federation, Russia

Keywords: Low-Count Image Reconstruction, Quantum Noise, Image Perception Quality, Retinex Model, Receptive Fields.

Abstract: The work is devoted to the issues of synthesizing a new method for low-count images reconstruction based on a realistic distortion model associated with quantum (Poisson) noise. The proposed approach to the synthesis of the reconstruction methods is based on the principles and concepts of statistical learning, understood as input learning (cf. adaptive smoothing). The synthesis is focused on a special representation of images using sample of counts of controlled size (sampling representation). Based on the specifics of this representation, a generative model of an ideal image is formulated, which is then concretized to a probabilistic parametric model in the form of a system of receptive fields. This model allows for a very simple procedure for estimating the count probability density, which in turn is an estimate of the normalized intensity of the registered radiation. With the help of the latter, similarly to the scheme of wavelet thresholding algorithms, a procedure for extracting contrast in the image is built. From the perception point of view, the contrast carries the main information about the reconstructed image, so such a procedure would provide a high image perception quality. The contrast extraction is carried out by comparing the number of counts in the centre and in the concentric surround of ON/OFF receptive fields and turns out to be very similar to wavelet thresholding.


1 INTRODUCTION

Image reconstruction usually refers to the problem of converting sparse or incomplete data, such as, for example, radiation counts (readings) from computed tomography scans, into a readable and usable image. More generally, image reconstruction involves transforming some dataset that is difficult to interpret into an easier-to-interpret target image, where the target image is some physical property (reflectance, illumination, absorption), that can be a proxy for the layout and/or shape of any objects (Aykroyd, 2015).

With the development of imaging technology (in various radiation ranges, including terahertz, infrared, X-ray), as well as with the increase in memory capacity and data processing speed of both conventional computers and specialized processors, interest in image reconstruction methods is growing rapidly. Biomedicine is a clear illustration of this. Image reconstruction is used now in all popular medical imaging techniques: magnetic resonance imaging (MRI), computed tomography (CT),

radiography (X-ray scanning), etc. At the same time, since the diagnostic decisions and patient treatments are often based on digital images, the requirements for the quality of reconstruction in medicine are very high.

The imaging techniques listed above are the products of very different technologies, so their resulting images differ a lot. However, recently, more and more often most of them meet the same problem – formation of images under the conditions of weak radiation registration. These conditions can arise for various reasons: in the THz range – due to the lack of natural sources; in optical astrophysical imaging – because of the remoteness of objects; in the X-ray, for example, in CT – due to the desire to reduce radiation doses. However, since all these radiation types have a common physical (electromagnetic) nature, there are also common features that manifest themselves in the case of low intensities for all ranges. Namely, in all ranges, the weak radiation acquires a quantum character and the registration process – image forming – is carried out in the form of registration of

^a <https://orcid.org/0000-0002-6770-1317>

(photo) counts. A good discussion of various aspects of low-count images for various ranges and applications is contained in (Caucci, 2012) (see also the extensive bibliography there).

A characteristic feature of low-count images is the grainy structure of their textures. Often these distortions are referred to as quantum (photon) noise (Dougherty, 2009). Quantum noise degrades both spatial resolution and contrast, making images difficult to interpret. Thus, quantum noise also reduces the speed and accuracy of image processing, such as segmentation, contrast enhancement, edge detection, etc. In a good medical imaging system, inevitable quantum noise is a major source of random distortion.

Quantum noise manifests itself in the random nature of independent discrete counts, which are well described by the Poisson probability distribution. An important characteristic of the Poisson distribution is the fact that the standard deviation of the counts number is equal to the square root of their intensity (mean). It follows from this, that quantum noise – deviation of intensity is not additive with respect to the signal – intensity (in contrast to the traditional white Gaussian noise). So, quantum noise suppression by traditional linear filtering turned out to be ineffective.

Non-linear adaptive smoothing methods using median-type filters have proved to be more successful (Oulhaj, 2012). The general idea of adaptive smoothing is to apply a versatile averaging that adapts to local topography of the image. Namely, adaptive smoothing filters average the image not over the window, but only over that part of it where the image values differ from the median, for example, by not more than a certain threshold. The development of the ideas of adaptive smoothing has recently taken place in several strategies. The first direction is the non-linear filtration, such as homomorphic Wiener, median and bilateral (Tomasi, 1998) filtering. The second direction is Perona and Malik approach (Perona, 1990), known as anisotropic diffusion, which is based on Partial Differential Equations (PDE) and attempts to save edges and lines. The third direction – the total variation (TV) approach goes back to Rudin and Osher (Rudin, 1992) and is based on minimizing some energy (penalty) function. Slightly apart from these three strategies is the fourth one – the wavelet thresholding (wavelet compression) technique, proposed by Weaver (Weaver, 1991). Wavelet thresholding separates additive noise from the true image in the following three-step framework: *analysis* – the input data is transformed to wavelet scaling coefficients; *shrinkage* – a threshold is

applied individually to the wavelet coefficients and *synthesis* – the denoised version of image is obtained by back-transforming the modified wavelet coefficients.

Certain successes have been achieved in some of the listed strategies. So, it is possible to recommend special methods for specific applications. But in terms of universal application to a wide range of problems, almost all methods show approximately the same quality of image enhancement. Moreover, Weickert and colleagues showed that many of these methods can be reduced to one another, at least within the framework of their algorithmic realization (Alt, 2020). In this regard, in low-count image reconstruction, all these methods demonstrate approximately the same relatively low quality.

It seems that the mediocre quality of the reconstruction is related to the above noted problem – modelling of distortions by additive noise. The transition from the image additive global modelling in the classical filtration theory to local modelling in the adaptive smoothing methods really leads to an increase in the quality, but it does not become significant. Technically, this is due to the fact that the minimization of some (mathematical) metric of the difference between the resulting image and its original is taken as a quality criterion. The most used metrics here are the sums of absolute or quadratic differences between the low-count and reconstructed images. However, it is well known that the image distortion perceived by a human cannot be adequately described by such simple mathematical instruments (Blau, 2019). Since visual perception is very complex and subject to many distortion factors, the use of a simple metric for perception quality is hardly a promising way.

In this regard, it seems more justified to look for new approaches to improve the quality of images starting not from the classical methods of digital image processing (DiSP), but from a large amount of data accumulated in the field of psychophysics of vision (Werner, 2014), (Schiller, 2015). A large amount of data about the periphery of the visual system (retina) is systematized within the framework of the so-called Retinex model, first proposed by Edwin G. Land (Land, 1971). The modern concept of Retinex considers the illumination created by natural or artificial sources of radiation, and the reflectivity of certain objects that redirect this radiation to imaging devices (the eye, for example) as the main physical parameters of visual perception. The illumination usually varies smoothly over a wide range, so information associated with this factor is usually negligible. On the other hand, the sharp

changes in the reflection coefficient between some objects and at the objects edges are very informative, and in a sense constitute the main content of images for a person.

To date, several types of image contrast enhancement algorithms based on the Retinex model are known. These algorithms usually analyze an image at several scales, extracting a low space frequency component, interpreted as illumination, and a high frequency component, interpreted as reflectivity. Local contrast is enhanced by compressing the luminance range or by extracting the reflectance. Among the algorithms implemented in the spirit of Retinex, we note first of all Center/Surround Retinex (Jobson, 1997), which forms an adaptively smoothed log of image and subtracts it from the log of original image to increase contrast. The current state of the algorithm including its application in NN – RetinexNet can be found in (Hai, 2023).

In this article, we propose a new method for low-count images reconstruction based on a realistic distortion model associated with quantum (Poisson) noise. In contrast to the known approaches listed above, we propose a fundamentally different one – the perceptual reconstruction of images based on the most adequate representation model of the recorded data for human visual perception (not based on formal metrics of the difference between low-count and reconstructed images, such as Least-Squares etc). Namely, we substantiate our approach on the previously developed biologically motivated representation of image by controlled size sample of counts (sampling representation) (Antsiperov, 2023). Since sampling representations are random objects, the proposed approach is fundamentally statistical. Considering that a complete statistical description of sampling representation is a product of the probability distribution densities of individual counts, the goal of the proposed approach is, in essence, to estimate these densities. In this regard, it is extremely important to choose a model of parametric distribution densities adequate to the features of visual perception. In the next section we discuss in detail the choice of a parametric family in the form of a system of receptive fields and derive a density estimating procedure based on sampling representations in the proposed parametric model. Considering that the obtained density estimate is a random realization of the normalized radiation intensity, in the last section we synthesize a procedure for extracting the image contrast from the density. Contrast extraction is carried out by comparing the number of counts in the centre and in the concentric surround of ON/OFF

receptive fields. The procedure turns out to be very similar to wavelet thresholding (Weaver, 1991), but there are two differences. Instead of wavelets the receptive fields are used. Instead of the wavelet coefficients shrinkage to zero, the centre / surround counts number shrink to the average value between them is explored. In this regard, it should be emphasized once again that the methods and models proposed below are largely motivated by the mechanisms of the human visual system (HVS) (Antsiperov, 2022). The fact that they lead to procedures analogous to modern digital signal processing methods, most likely determine their success.

2 CENTRE/ SURROUND RETINEX-LIKE MODEL FOR LOW-COUNT IMAGES

The imaging modalities listed above (MRI, CT, X-ray, etc.) are based on very different technologies, deal with significantly different types of images, and are ultimately intended for different applications. However, since they all are representatives of the same electromagnetic radiation, they can be described by the same (parametric) model by choosing definite parameters (wavelength/frequency) for each range. This is also true in the case of weak working radiation, with the only refinement that the model of radiation–matter interaction should be more accurately described in the frames of quantum theory.

The discussion of the adequate model for detecting weak radiation and its substantiation within the framework of a semiclassical description can be found, for example, in (Antsiperov, 2021). The main feature of this model in comparison with the classical description is that the registration of weak radiation forming an image results in a set of random (photo) counts. Thus, the representation of an image by counts is essentially random, in contrast to the classical case, where randomness is associated with external (additive) noise. The statistical description of such a representation can be given by using the concept of an ideal imaging device (Antsiperov, 2023). The latter is a plain array (matrix) of ideal point detectors (cf. jots – (Fossum, 2020)). So, the result of registration of the photon flux incident on the sensitive surface Ω of an ideal imaging device is a set of counts $X = \{\vec{x}_i\}$, where \vec{x}_i , $i = 1, \dots, N$ are the coordinates of the registered photons – random vectors in some area Ω of the plain \mathbb{R}^2 . Note that the

number of registered counts N is also a random variable.

It is easy to show (Antsiperov, 2021) that the statistics of random N is given by the Poisson distribution with the mean parameter \bar{N} :

$$\bar{N} = \alpha T \int_{\Omega} I(\vec{x}) d\vec{x}, \quad \alpha = \eta/h\bar{\nu} \quad (1)$$

where $I(\vec{x})$ is the intensity of radiation incident on the sensitive surface Ω , T is the registration time, η is the ideal imaging device quantum efficiency, h is the Planck's constant and $\bar{\nu}$ is some characteristic radiation frequency. Further, it is relatively easy to show (Streit, 2010.) that the set of counts $X = \{\vec{x}_i\}$ can be statistically described as a probability distribution of points \vec{x}_i of some two-dimensional inhomogeneous Poisson point process (PPP) with the intensity function $\nu(\vec{x}) = \alpha T I(\vec{x})$, proportional to the registered radiation intensity.

Since the number of counts N is a random variable, the above description is not convenient for practical use (especially if N is large enough). Therefore, we proposed a representation of low-count images by sets of random vectors, like a set of Poisson points, but with a fixed (controlled) total number $n \ll N$. Namely, considering the complete set of counts $X = \{\vec{x}_i\}$ of an ideal imaging device as some general population and making a random sample of n counts from it $X_n = \{\vec{x}_{ij}\}$, $j = 1, \dots, n$, we consider the latter as the desired representation of the image, called sampling representation. The statistical discussion of the sampling from the finite population can be found in (Wilks, 1962). We have shown (Antsiperov, 2023) that under the same assumptions that were used to derive the PPP statistics, the statistics of a fixed (non-random) size n sample X_n can be given by a conditional (for a given image $I(\vec{x})$) multivariate distribution density of the form:

$$\begin{aligned} \rho(X_n = \{\vec{x}_j\}, | I(\vec{x})) &= \prod_{j=1}^n \rho(\vec{x}_j | I(\vec{x})), \\ \rho(\vec{x}_j | I(\vec{x})) &= \frac{I(\vec{x}_j)}{\int_{\Omega} I(\vec{x}) d\vec{x}}. \end{aligned} \quad (2)$$

where, by means of $\vec{x}_j = \vec{x}_{ij}$, $j = 1, \dots, n$, the indexing of counts, internal for the sampling representation X_n , is introduced.

To illustrate typical realizations of random counts for real images and to prepare sampling representation examples for further processing, we generated, in accordance with (2), three sets of X_n counts: one for simple artificial image ("slope") and a pair for images ("apple-1" and "beetle-8") from the standard data set MPEG7 Core Experiment CE-

Shape-1 (Latecki, 2000), which are presented in Figure 1.

All the three images were converted to PNG format with a color depth of $\nu = 8$ bits (greyscale) and an image size of $s \times s = 1200 \times 1200$ pixels. Wherein only two shades of grey were used for each image. Counts were generated by the Monte-Carlo accept-reject method (Robert, 2004) with a uniform auxiliary distribution $g(\vec{x}) = (s \times s)^{-1} = 1200^{-2}$ and an auxiliary constant M equal to the largest value of pixels $2^{\nu} = 256$ (see details in (Antsiperov, 2023)).

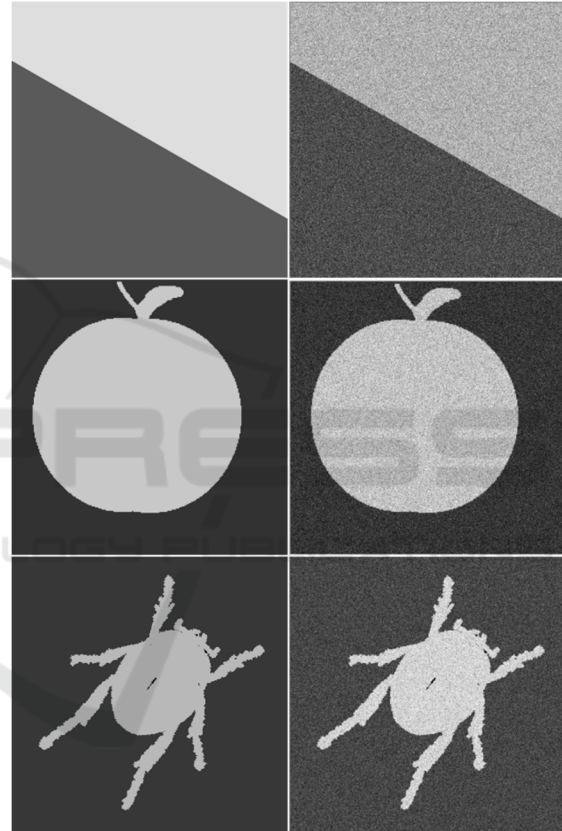


Figure 1: Image representations by samples of counts (sampling representations). Left column – source images "slope", "apple-1" and "beetle-8" (Latecki, 2000). Right column – corresponding sampling representations, each with a size of 3 000 000 counts.

With regard to visual perception, it can be assumed that the proposed sampling representation of images is quite consistent with the data recorded by discrete photoreceptors (rods, cones) at the input of the visual system – in the outer layer of the retina (Antsiperov, 2023). At the same time, it is important to emphasize that the nerve impulses (spikes) sent to the brain from retina are not the same as the data

directly recorded by photoreceptors. Retinal ganglion cells (RGS) – the neurons in the inner layer of retina, whose axons compose the optic nerve, perform the retina's output with the help of numerous intermediate neurons of the middle and inner layers. Among them, in addition to bipolar cells that bind receptors and RGCs from the outer to the inner layer, horizontal and amacrine cells play an important role, making horizontal connections in the layers. As a result, each ganglion cell can receive and process signals from dozens and sometimes thousands of receptors. In this regard, it seems that the retina performs a rather complex processing of input data, aimed primarily at their optimal compression. Indeed, if we consider that the number of retinal receptors reaches $\sim 10^8$, and the number of axons of the optic nerve is only 10^6 (Schiller, 2015), the amount of input data is compressed in size by a factor of one hundred. So, because the retina compresses the input data, image analysis at higher levels of the visual system will require its reconstruction. The modern point of view on the optimization of these related processes is that the synthesis of the corresponding procedures should essentially rely on carefully and appropriately modelling of the available mechanisms / structures.

Explicit use of statistical descriptions and probabilistic models is the main distinguishing feature of statistical image reconstruction compared to classical deterministic methods. Statistical reconstruction provides both a flexible relationship between data and parameters, described by a likelihood, and relationships between parameters described by prior distributions. The key concept that combines both descriptions is the Bayes theorem (Aykroyd, 2015). At the same time, even within the Bayesian framework, successful approaches can be developed that differ significantly from each other. Today, for example, in modern DiSP, an original idea has been developed that for reconstruction problems not only traditional methods that *a priori* model image parameters (classical Bayesian methods), but also the methods modelling image features based on the data of the images themselves (empirical Bayesian methods) can be successfully used. (Milanfar, 2013). Further discussion is devoted to the implementation of this idea in the reconstruction problem considered.

Since by the image we mean the registered intensity $I(\vec{x})$, the first question of the image modelling is thus the choice of a model for the intensity. Let us assume that the intensity can be modelled by a set of parameters $\vec{\theta} \in \theta \subset \mathbb{R}^p$, which describe some of its features. Temporarily, without specifying the content of these features, we assume

that such a p -dimensional parametric model $I(\vec{x}; \vec{\theta})$ is chosen. According (2), this model can be reduced to the parametric model of the count probability distribution $\rho(\vec{x}_i | I(\vec{x})) = \rho(\vec{x}_i; \vec{\theta})$. Thus, the image encoding (compression) can be reduced to the parameters $\vec{\theta} \in \theta$ estimation, based on the sampling representation $X_n = \{\vec{x}_i\}$, which, again according to (2), is given by the product of the densities of individual counts:

$$\rho(X_n; \vec{\theta}) = \prod_{i=1}^n \rho(\vec{x}_i; \vec{\theta}) \quad (3)$$

It follows from (3) that for image modelling it is necessary and sufficient to determine the type of parametric model $\mathbb{P} = \{\rho(\vec{x}; \vec{\theta}) | \vec{\theta} \in \theta\}$ of distribution density of count. To concretize this model, it needs, as noted above, to appropriately adapt it to the known data from the subject area. Following the initially chosen orientation to the mechanisms / structures of the visual system, we formalize for these purposes a perceptually motivated image model \mathbb{P} . This model is associated primarily with the concept of retinal receptive fields (Schiller, 2015), therefore, to substantiate the model, we recall some basic facts about the mechanisms of neural encoding at the HVS periphery (retina).

Starting from the works of Hubel and Wiesel in the 1960s (Hubel 2004), the structure and functions of retinal receptive fields (RFs) have been studied quite deeply (Schiller, 2015). The functions and sizes of individual RFs are determined by the types of ganglion cells associated with them (retinal output neurons). The number of types of the latter exceeds ~ 20 , but most of them ($\sim 80\%$) belong to two main types – midget and parasol cells, each of which has two subtypes – ON- and OFF-cells. In order not to overload the discussion, we will further consider only the family of midget cells encoding the spatial intensity distribution in the image. Subtypes of ON- and OFF-cells differ in their response to the nature of illumination/darkening of the corresponding RFs in accordance with the central antagonistic structure of the latter. ON-cells are activated upon stimulation of the RF center and inhibited upon stimulation of the concentric surround. Conversely, OFF-cells are activated upon stimulation of the RF surround and inhibited upon stimulation of the center (Schiller, 2015). In known mathematical models, the receptive field of an ON- cell has a center (C) in the form of a narrow Gaussian profile of spatial activation of photoreceptors and a wider concentric profile of inhibition in an antagonistic surround (S); for OFF-cells, activation and inhibition are reversed. This type

of model is commonly referred to as DoG (difference of Gaussian) (Cho, 2014).

As for the spatial arrangement of the system of receptive fields, it was found that some pairs of ON- and OFF-cells have almost completely overlapped RFs, while the fields of different pairs practically do not overlap. At the same time, non-overlapping pairs of adjacent RFs closely adjoin each other, forming a kind of mosaic that densely fills the entire field of view Ω of the retina (Gauthier, 2009), see Figure 2.

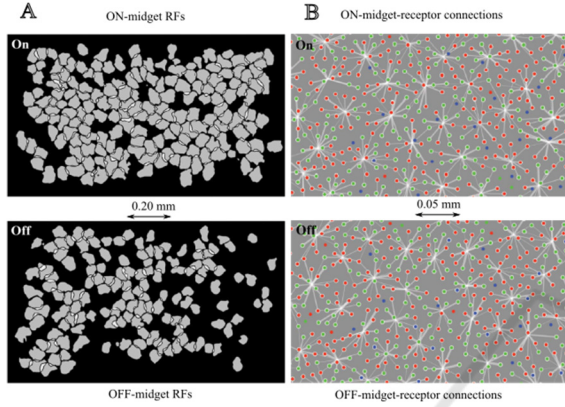


Figure 2: Locations and shapes of RFs in large populations of ON- and OFF-midget cells on the retina surface. A) The RFs of ON- and OFF-cells as a regularly spaced mosaic, represented by a collection of contour lines. B) The RFs of ON- and OFF-cells as a connection with the receptors identified in a single recording of the cell sampling. Adapted from (Gauthier, 2009) and (Field, 2010).

Based on the previous short overview, we formalize the parametric model of the family of count probability densities $\mathbb{P} = \{\rho(\vec{x}; \vec{\theta}) | \vec{\theta} \in \Theta\}$ as a mixture of K pairs of components $\{C_k(\vec{x}), S_k(\vec{x})\}$, $k = 1, \dots, K$:

$$\rho(\vec{x}; \vec{\theta}) = \sum_{k=1}^K w_k C_k(\vec{x}) + v_k S_k(\vec{x}) \quad (4)$$

where $\vec{\theta} = \{w_k, v_k\}$ are positive mixture weights, the model \mathbb{P} parameters and mixture components $C_k(\vec{x})$ and $S_k(\vec{x})$ represent compact center and antagonistic surround of the k -th pair of ON/OFF receptive fields. Components $C_k(\vec{x})$ and $S_k(\vec{x})$ are given by positive probability distribution densities, having compact supports $\Delta_k^c = \{\vec{x} | C_k(\vec{x}) > 0\}$ and $\Delta_k^s = \{\vec{x} | S_k(\vec{x}) > 0\}$, composing in the sum the general support of the k -th RF pair: $\Delta_k = \Delta_k^c \cup \Delta_k^s$:

$$\int_{\Delta_k^c} C_k(\vec{x}) d\vec{x} = \int_{\Delta_k^s} S_k(\vec{x}) d\vec{x} = 1 \quad (5)$$

If we assume that the supports Δ_k^c and Δ_k^s do not intersect each other: $\Delta_k^c \cap \Delta_k^s = \emptyset$, then we can add

the orthogonality-like relations to the normalization-like equations (5):

$$\int_{\Delta_k^c} S_k(\vec{x}) d\vec{x} = \int_{\Delta_k^s} C_k(\vec{x}) d\vec{x} = 0 \quad (6)$$

Further, we assume that the set of RF supports $\{\Delta_k\}$ constitutes a partition (mosaic) of the overall surface of the retina, i.e., all $\{\Delta_k\}$ are pairwise disjoint, but together they densely cover Ω . This RFs property causes the components to disappear on all supports Δ_l that do not contain their own Δ_k :

$$C_k(\vec{x}) = S_k(\vec{x}) = 0, \quad \vec{x} \in \Delta_l, k \neq l \quad (7)$$

Relations (5, 6, 7) make it very easy to express the parameters $\vec{\theta} = \{w_k, v_k\}$ of the model in terms of corresponding integrals of the probability density $\rho(\vec{x}; \vec{\theta})$ (4) over the corresponding supports and thereby clarify the nature of the parameters as the probabilities of hitting counts to some centres Δ_k^c or surrounds Δ_k^s of receptive fields:

$$\begin{aligned} w_k &= \int_{\Delta_k^c} \rho(\vec{x}; \vec{\theta}) d\vec{x} \\ v_k &= \int_{\Delta_k^s} \rho(\vec{x}; \vec{\theta}) d\vec{x} \end{aligned} \quad (8)$$

Let us make the following remark regarding (8). Expressions (8) characterize w_k and v_k also as the mean values of the characteristic functions $\Pi_k^c(\vec{x}) = 1$ if $\vec{x} \in \Delta_k^c$, else 0 and $\Pi_k^s(\vec{x}) = 1$ if $\vec{x} \in \Delta_k^s$, else 0 on the surface Ω .

Obviously, expressions (3) cannot be used to find w_k and v_k , since the probability density $\rho(\vec{x}; \vec{\theta})$ of image is not known, but only its sampling representation $X_n = \{\vec{x}_j\}$ is available. However, given the number of image counts, one can use the standard trick, described, for example, in (Donoho, 1994), for estimating the probability density by wavelet decomposition with empirically formed coefficients. So, keeping in mind the asymptotic of the large numbers law and replacing the means of $\Pi_k^c(\vec{x})$ and $\Pi_k^s(\vec{x})$ by their sample (empirical) means, we can approximately write:

$$\begin{aligned} w_k &= \frac{1}{n} \sum_{j=1}^n \Pi_k^c(\vec{x}_j) = \frac{n_k^c}{n}, \\ v_k &= \frac{1}{n} \sum_{j=1}^n \Pi_k^s(\vec{x}_j) = \frac{n_k^s}{n}. \end{aligned} \quad (9)$$

where n_k^c and n_k^s are the numbers of counts in the center and in the surround of the corresponding RFs.

It is easy to show that, within the framework of the assumptions made ($\Omega = \bigcup_{k=1}^K \Delta_k$, $\Delta_k \cap \Delta_l = \emptyset$, $k \neq l$, $\Delta_k = \Delta_k^c \cup \Delta_k^s$, $\Delta_k^c \cap \Delta_k^s = \emptyset$), the parameters w_k and v_k (9) are indeed a probability distribution in

full accordance with the above interpretation: they all are non-negative and satisfy the normalization condition:

$$\sum_{k=1}^K (w_k + v_k) = \frac{1}{n} \sum_{k=1}^K n_k = 1 \quad (10)$$

where $n_k = n_k^c + n_k^s$ is the number of counts in sample X_n hitting the common support $\Delta_k = \Delta_k^c \cup \Delta_k^s$ of the center and surround of k -th RF. Note that the solutions (9) do not depend at all on the forms of $C_k(\vec{x})$ and $S_k(\vec{x})$, but only on the forms of their supports Δ_k^c and Δ_k^s (namely, from the number of counts that fell into their boundaries). Hence it follows that for an approximate estimate of the probability density $\rho(\vec{x}; \vec{\theta})$ (4) only the numbers n_k^c and n_k^s of counts in the centers / surrounds of the receptive fields are sufficient. In other words, the sampling representation $X_n = \{\vec{x}_j\}$ of image can be reduced in the case considered to occupation number representation $Y_n = \{n_k^c, n_k^s\}$.

3 CENTRE/SURROUND RETINEX SHRINKAGE

As noted above, both the chosen model (8) and the resulting image encoding procedure (9) are very similar to the wavelet decomposition. In fact, the very idea of finding the decomposition weights (9) as sample means was motivated by the Donoho and Johnstone in work (Donoho, 1994), devoted to selective wavelet reconstruction.

In this regard, a natural question arises: why, continuing the noted analogy, not to try applying to the problem under consideration the most successful methods from the field of wavelet analysis, considered as a variant of multiresolution analysis (Mallat, (1989).)? Of course, the wavelet thresholding methods (Weaver, 1991) that are extremely popular today and often cited as wavelet shrinkage methods (Alt, 2020), should be noted among them first. Thus, concretizing the previous question, we can formulate the following problem: considering procedure (9) as the first step – *analysis* in some RF thresholding method – construct its subsequent steps by analogy with the wavelet shrinkage method (see Introduction).

For this, by the way, there are strong reasons. Namely, as emphasized in (Chipman, 1997), the main reason for the use of wavelet shrinkage for some signal denoising problem is the sparseness of its underlying set of fine-scale coefficients. That is, if most of these coefficients are small, and a few remaining coefficients are large, then only they

explain most of the signal form. By shrinking the coefficients toward 0, the smaller ones (which contain primarily noise) may be reduced to negligible levels, hence denoising the signal. In methods based on the Retinex model, a similar strategy is utilized – the local contrast enhancement by compressing smooth luminance variations and extract sharp changes of the reflectance. Several successful algorithms (Jobson, 1997) implement this strategy based on Center/Surround mechanism for estimating the degree of sharpness of intensity changes. Below, we propose our own version of a similar approach.

In the frames of approximations (9) made, the nature of the representation $Y_n = \{n_k^c, n_k^s\}$ remains random, so the density estimation (4) could be still very noisy. To improve its quality some *a priori* information about the parameters (in this case $\{n_k^c, n_k^s\}$) should be used. However, unlike the method of wavelet compression, based on a simple additive (linear) model of Gaussian noise, the noise in our model is multiplicative. These circumstances significantly complicate the analysis of statistical relationships and the synthesis of the reconstructing procedure in the chosen model. Nevertheless, we succeeded in synthesizing a new Retinex-like Center/Surround reconstruction method, which has the form of parameters $Y_n = \{n_k^c, n_k^s\}$ correction for the optimal estimates $\bar{Y}_n = \{\bar{n}_k^c, \bar{n}_k^s\}$ calculation to *synthesize* the smoothed the count distribution density $\rho(\vec{x}; \vec{\theta})$ (4).

Since the parameters n_k^c, n_k^s are independent on different RFs, the analysis of their statistics can be carried out independently for all such fields. So, let us consider some of such fields and denote its non-negative numbers of counts at center by n_c and at antagonistic surround – by n_s . As this random numbers have the Poisson distribution, their expectations are $n_c = \sigma_c \lambda$ and $n_s = \sigma_s \mu$, where λ is the intensity of counts at the center of RF, and μ is the intensity of counts at surround, σ_c and σ_s are the areas of the center and surround, so $\sigma = \sigma_c + \sigma_s$ is the area of RF support Δ . So, the probabilistic model of n_c, n_s has the form:

$$\begin{aligned} n_c | \lambda &\sim \pi(n_c | \sigma_c \lambda) = \frac{(\sigma_c \lambda)^{n_c}}{n_c!} \exp\{-\sigma_c \lambda\}, \\ n_s | \mu &\sim \pi(n_s | \sigma_s \mu) = \frac{(\sigma_s \mu)^{n_s}}{n_s!} \exp\{-\sigma_s \mu\}. \end{aligned} \quad (11)$$

It follows from (11) that the total number of counts $n = n_c + n_s$ is also Poissonian:

$$n | \lambda, \mu \sim \pi(n | \sigma_c \lambda + \sigma_s \mu) = \frac{(\sigma_c \lambda + \sigma_s \mu)^n}{n!} \exp\{-(\sigma_c \lambda + \sigma_s \mu)\} \quad (12)$$

If a *priori* model of parameters λ, μ is $\rho(\lambda, \mu)$, then overall generative model (joint distribution of n_c, n_s and parameters λ, μ) according (11) is:

$$\begin{aligned} \rho(n_c, n_s, \lambda, \mu) &= \rho(n_c, n_s | \lambda, \mu) \rho(\lambda, \mu) = \\ &= \pi(n_c | \sigma_c \lambda) \pi(n_s | \sigma_s \mu) \rho(\lambda, \mu) = \\ &= \frac{(\sigma_c \lambda)^{n_c} (\sigma_s \mu)^{n_s}}{n_c! n_s!} \exp \{-(\sigma_c \lambda + \sigma_s \mu)\} \rho(\lambda, \mu) \end{aligned} \quad (13)$$

Using (12) one can rewrite (13) as

$$\begin{aligned} \rho(n_c, n, \lambda, \mu) &= \\ &= C_n^{n_c} \left(\frac{\sigma_c \lambda}{\sigma_c \lambda + \sigma_s \mu} \right)^{n_c} \left(\frac{\sigma_s \mu}{\sigma_c \lambda + \sigma_s \mu} \right)^{n-n_c} \times \\ &\times \pi(n | \sigma_c \lambda + \sigma_s \mu) \rho(\lambda, \mu) \end{aligned} \quad (14)$$

We choose a *priori* model $\rho(\lambda, \mu)$ as a mixture of two components:

$$\rho(\mu, \lambda) = p \delta(\mu - \lambda) \wp(\lambda) + (1-p) \wp(\mu) \wp(\lambda), \quad (15)$$

where the hyperparameter p can be treated as the probability of the hypothesis H_0 that μ and λ coincide.

If follows from (15), that marginal (unconditional) distributions of λ and μ are

$$\begin{aligned} \rho(\mu) &= p \wp(\mu) + (1-p) \wp(\mu) = \wp(\mu) \\ \rho(\lambda) &= p \wp(\lambda) + (1-p) \wp(\lambda) = \wp(\lambda) \end{aligned} \quad (16)$$

Note that the marginal distributions (16) do not depend on the hypotheses $H_0, \overline{H_0}$ and both are given by the unconditional distribution $\wp()$.

On the base of (15), (16) we obtain, that conditional distributions of parameters λ, μ under $H_0, \overline{H_0}$ have the form:

$$\begin{aligned} \rho(\mu, \lambda | H_0) &= \\ &= \rho(\mu | \lambda, H_0) \rho(\lambda | H_0) = \delta(\mu - \lambda) \wp(\lambda), \\ \rho(\mu, \lambda | \overline{H_0}) &= \\ &= \rho(\mu | \lambda, \overline{H_0}) \rho(\lambda | \overline{H_0}) = \wp(\mu) \wp(\lambda) \end{aligned} \quad (17)$$

As follows from (17), in contrast to (16), the conditional distributions λ and μ do depend on hypotheses $H_0, \overline{H_0}$, since $\rho(\mu | \lambda, H_0) = \delta(\mu - \lambda)$ and $\rho(\mu | \lambda, \overline{H_0}) = \wp(\mu)$. Nevertheless, it is interesting that under the hypothesis $\overline{H_0}$ the parameters λ, μ are still independent.

Substituting model (15) into (13), we obtain the following expressions for joint distribution (likelihood function):

$$\begin{aligned} \rho(n_c, n_s, \lambda, \mu) &= \\ &= p C_n^{n_c} \left(\frac{\sigma_c}{\sigma} \right)^{n_c} \left(\frac{\sigma_s}{\sigma} \right)^{n_s} \times, \\ &\times \pi(n | \sigma \lambda) \wp(\lambda) \delta(\mu - \lambda) + \\ &+ (1-p) \pi(n_c | \sigma_c \lambda) \wp(\lambda) \pi(n_s | \sigma_s \mu) \wp(\mu) \end{aligned} \quad (18)$$

where $C_n^{n_c} = n! / n_c! (n - n_c)!$ – binomial coefficient, $\sigma = \sigma_c + \sigma_s$, $n = n_c + n_s$. By integrating (18) over λ and μ from 0 to ∞ , we obtain the (unconditional) joint distribution of n_c and n_s :

$$\begin{aligned} \rho(n_c, n_s) &= \\ &= p C_n^{n_c} \left(\frac{\sigma_c}{\sigma} \right)^{n_c} \left(\frac{\sigma_s}{\sigma} \right)^{n_s} P_\sigma(n) + \\ &+ (1-p) P_{\sigma_c}(n_c) P_{\sigma_s}(n_s) \end{aligned} \quad (19)$$

where probability distribution $P_\sigma(n)$ of integer n is

$$\begin{aligned} P_\sigma(n) &= \int_0^\infty \pi(n | \sigma \lambda) \wp(\lambda) d\lambda = \\ &= \int_0^\infty \frac{(\sigma \lambda)^n}{n!} \exp\{-\sigma \lambda\} \wp(\lambda) d\lambda \end{aligned} \quad (20)$$

If $\wp(\lambda)$ is a smooth function at n/σ on a scale $\sim \sqrt{n}/\sigma$, then a good approximation can be written for distribution (20):

$$P_\sigma(n) \approx \frac{1}{\sigma} \wp\left(\frac{n}{\sigma}\right). \quad (21)$$

From (18) it follows that conditional joint distributions of n_c and n_s are

$$\begin{aligned} \rho(n_c, n_s | H_0) &= C_n^{n_c} \left(\frac{\sigma_c}{\sigma} \right)^{n_c} \left(\frac{\sigma_s}{\sigma} \right)^{n_s} P_\sigma(n), \\ \rho(n_c, n_s | \overline{H_0}) &= P_{\sigma_c}(n_c) P_{\sigma_s}(n_s). \end{aligned} \quad (22)$$

So, according to (22), for a given $n = n_c + n_s$, the distribution of numbers n_c, n_s under the hypothesis H_0 is binomial and under $\overline{H_0}$ n_c, n_s are independent.

If with the help of (A.10) we introduce the likelihood ratio of hypotheses $H_0, \overline{H_0}$

$$\begin{aligned} A_n^{n_c} &= \frac{\rho(n_c, n_s | H_0)}{\rho(n_c, n_s | \overline{H_0})} = \\ &= C_n^{n_c} \left(\frac{\sigma_c}{\sigma} \right)^{n_c} \left(\frac{\sigma_s}{\sigma} \right)^{n_s} \frac{P_\sigma(n)}{P_{\sigma_c}(n_c) P_{\sigma_s}(n_s)} \end{aligned} \quad (23)$$

(18) and (19) will give us the following expression for the posterior distribution:

$$\begin{aligned} \rho(\lambda, \mu | n_c, n_s) &= \\ &= \frac{\frac{p}{1-p} A_n^{n_c} \frac{\pi(n | \sigma \lambda)}{P_\sigma(n)}}{1 + \frac{p}{1-p} A_n^{n_c}} \wp(\lambda) \delta(\mu - \lambda) + \\ &+ \frac{\frac{\pi(n_c | \sigma_c \lambda)}{P_{\sigma_c}(n_c)} \frac{\pi(n_s | \sigma_s \mu)}{P_{\sigma_s}(n_s)}}{1 + \frac{p}{1-p} A_n^{n_c}} \wp(\lambda) \wp(\mu) \end{aligned} \quad (24)$$

Calculating the first moments of distribution (24) in the usual way, we can obtain the conditional (for a given n_c and n_s / n) expected values $\bar{\mu}$ and $\bar{\lambda}$ of parameters μ and λ . Since the result is, although simple, but cumbersome expressions, let us use the assumptions made in the derivation of approximation (21), which allow us to set

$$\frac{P_{\sigma}(n+1)}{P_{\sigma}(n)} \approx \frac{\wp((n+1)/\sigma)}{P_{\sigma}(n/\sigma)} \approx 1 \quad .$$

and the same for ratios $P_{\sigma_c}(n_c + 1)/P_{\sigma_c}(n_c)$ and $P_{\sigma_s}(n_s + 1)/P_{\sigma_s}(n_s)$, and write down only the approximate result:

$$\begin{aligned} \bar{\lambda} &\approx \frac{\frac{p}{1-p} \Lambda_n^{n_c}}{1 + \frac{p}{1-p} \Lambda_n^{n_c}} \frac{n+1}{\sigma} + \frac{1}{1 + \frac{p}{1-p} \Lambda_n^{n_c}} \frac{n_c+1}{\sigma_c} \\ \bar{\mu} &\approx \frac{\frac{p}{1-p} \Lambda_n^{n_c}}{1 + \frac{p}{1-p} \Lambda_n^{n_c}} \frac{n+1}{\sigma} + \frac{1}{1 + \frac{p}{1-p} \Lambda_n^{n_c}} \frac{n_s+1}{\sigma_s} \end{aligned} \quad (25)$$

It follows from (25) that expected values $\bar{\mu}$ and $\bar{\lambda}$ are the weighed means of $(n+1)/\sigma$ and $(n_c+1)/\sigma_c$ or $(n_s+1)/\sigma_s$, which can be interpreted as average count densities on supports $\Delta = \Delta^c \cup \Delta^s$ and Δ^c or Δ^s of any RF. In two extreme cases – large $\Lambda_n^{n_c} p / (1-p) \gg 1$ and small $\Lambda_n^{n_c} p / (1-p) \ll 1$ expressions (25) for $\bar{\mu}$ and $\bar{\lambda}$ are even more simplified:

$$\begin{aligned} \bar{\lambda} &\approx \begin{cases} \frac{n+1}{\sigma_c + \sigma_s}, & \Lambda_n^{n_c} \gg \frac{(1-p)}{p} \\ \frac{n_c+1}{\sigma_c}, & \Lambda_n^{n_c} \ll \frac{(1-p)}{p} \end{cases} \\ \bar{\mu} &\approx \begin{cases} \frac{n+1}{\sigma_c + \sigma_s}, & \Lambda_n^{n_c} \gg \frac{(1-p)}{p} \\ \frac{n_s+1}{\sigma_s}, & \Lambda_n^{n_c} \ll \frac{(1-p)}{p} \end{cases} \end{aligned} \quad (26)$$

It follows from (26) that the dominating terms in the expected $\bar{\lambda}$ and $\bar{\mu}$ (25) are essentially determined by the value of likelihood ratio $\Lambda_n^{n_c}$ (23). When it is large enough (when the likelihood of hypothesis H_0 is larger than the likelihood of \bar{H}_0 in $(1-p)/p$ times) both the expected intensities $\bar{\lambda}$ and $\bar{\mu}$ are equal to total number of counts n (plus one) divided by the area σ of RF base support. Otherwise (when the likelihood of hypothesis H_0 is smaller than the likelihood of \bar{H}_0 in $(1-p)/p$ times) expected intensities $\bar{\lambda}$ and $\bar{\mu}$ are equal to their own ratios $(n_c+1)/\sigma_c$ and $(n_s+1)/\sigma_s$.

To simplify the boundary between the above extreme cases, let us consider the approximation of $\Lambda_n^{n_c}$ (23) in the case $n_c, n_s \gg 1$, whence it follows it also follows that $n = n_c + n_s \gg 1$. So, introducing the notations $\delta_c = \sigma_c/\sigma$ and $\delta_s = \sigma_s/\sigma$, $\delta_c + \delta_s = 1$, putting in these notations $n_c = \delta_c n + \varepsilon$, $n_s =$

$\delta_s n - \varepsilon$, where $\varepsilon = n_c - \delta_c n = \delta_s n - n_s$, and using the Stirling formula $n! \approx \sqrt{2\pi n} n^n \exp\{-n\}$, we get:

$$\Lambda_n^{n_c} \approx \frac{1}{\sqrt{2\pi n \delta_c \delta_s}} \exp\left\{-\frac{\varepsilon^2}{2n \delta_c \delta_s}\right\} \frac{\sigma_c \sigma_s}{\sigma \wp\left(\frac{\varepsilon}{\sigma}\right)} \quad (27)$$

where approximation (21) was used for $P_{\sigma}(n), P_{\sigma_c}(\delta_c n), P_{\sigma_s}(\delta_s n)$. So, in the case $n_c, n_s \gg 1$ the criterion $\Lambda_n^{n_c} \geq (1-p)/p$ boils down to the test:

$$\mathcal{F}(n_c | \delta_c n, \sqrt{n \delta_c \delta_s}) \geq \frac{(1-p)}{p} \frac{P_{\sigma}(n)}{\delta_c \delta_s} \quad (28)$$

where \mathcal{F} is the Gaussian distribution. After rearranging the factors and taking the logarithm, the test (28) becomes:

$$\frac{(n_c - \hat{n}_c)^2}{2n \delta_c \delta_s} \geq \ln \frac{p \sqrt{\delta_c \delta_s}}{\sqrt{2\pi(1-p)} P_{\sigma}(n)} \quad (29)$$

where $\hat{n}_c = \delta_c n$ is the estimate of n_c by the value of n under the assumption that the H_0 is valid and it is also taken into account that $n \gg \ln n$ when $n \gg 1$. If $\wp(\lambda)$ is almost uniform distribution, then $P_{\sigma}(n) \approx P_{\sigma}(0)$ does not depend on n and we can introduce not depending on n threshold:

$$D = \sqrt{2\delta_c \delta_s \ln \frac{p \sqrt{\delta_c \delta_s}}{\sqrt{2\pi(1-p)} P_{\sigma}(0)}} \quad (30)$$

which is determined by *a priori* data only.

Taking into account the above simplifications, the parameters correction problem (36) can be finally rewritten as:

$$\begin{aligned} \bar{\lambda} &\approx \begin{cases} \frac{n+1}{\sigma}, & |n_c - \hat{n}_c| < D\sqrt{n} \\ \frac{n_c+1}{\sigma_c}, & |n_c - \hat{n}_c| > D\sqrt{n} \end{cases} \\ \bar{\mu} &\approx \begin{cases} \frac{n+1}{\sigma}, & |n_c - \hat{n}_c| < D\sqrt{n} \\ \frac{n_s+1}{\sigma_s}, & |n_c - \hat{n}_c| > D\sqrt{n} \end{cases} \end{aligned} \quad (31)$$

To re-estimate model parameters $\vec{\theta} = \{w_k, v_k\}$, $w_k = n_k^c/n$ and $v_k = n_k^s/n$ (9), we can use the above results of Bayesian RF shrinkage as follows ($\hat{n}_k^c = \frac{\sigma_c}{\sigma} n_k$):

$$\begin{aligned} \tilde{w}_k &= \frac{\hat{n}_k^c}{n} \approx \begin{cases} \frac{n_k+1}{n} \frac{\sigma_c^k}{\sigma^k}, & |n_k^c - \hat{n}_k^c| < D\sqrt{n_k} \\ \frac{n_k^c+1}{n}, & |n_k^c - \hat{n}_k^c| > D\sqrt{n_k} \end{cases} \\ \tilde{v}_k &= \frac{\hat{n}_k^s}{n} \approx \begin{cases} \frac{n_k+1}{n} \frac{\sigma_s^k}{\sigma^k}, & |n_k^c - \hat{n}_k^c| < D\sqrt{n_k} \\ \frac{n_k^s+1}{n}, & |n_k^c - \hat{n}_k^c| > D\sqrt{n_k} \end{cases} \end{aligned} \quad (32)$$

4 IMAGES RECONSTRUCTION/ SYNTHESIS BASED ON RF SHRINKAGE

In order to illustrate the potential possibilities of the proposed approach, we carried out, basing on the procedure (32), the RF shrinkage of the images shown in Figure 1 and perform subsequent synthesis.

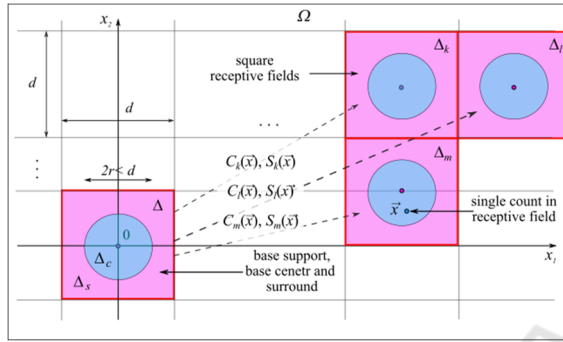


Figure 3: The image surface Ω partition by RF supports $\{\Delta_k\}$ in numerical RF shrinkage procedure implementation.

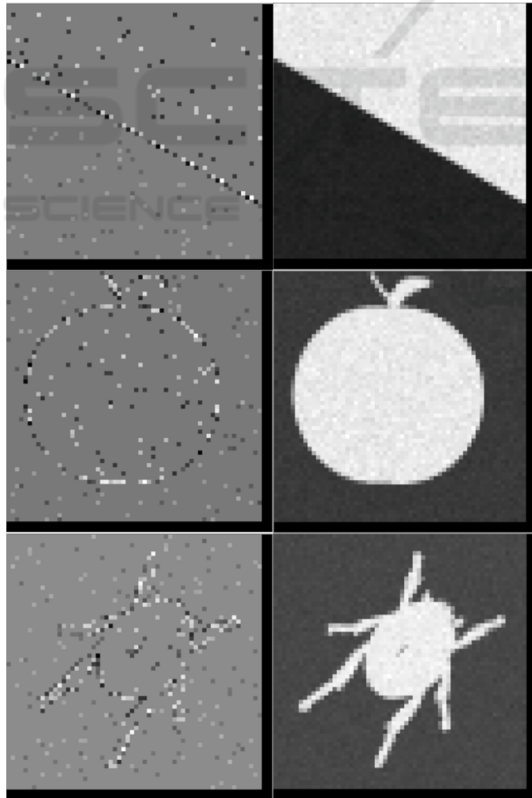


Figure 4: The contrast (sharp changes in the reflection coefficient) and smoothed version (slow changes in the illumination) of Figure 1 images. Left column – contrast (\tilde{n}_k^c), right column – smoothed version ($n_k + 1$), see (32).

In the numerical implementation of the procedure the image field Ω was divided into $K = L \times M$ square "receptive" fields $\{\Delta_k\}$, each of sizes $d \times d$ pixels (the original images had, respectively, the sizes $dL \times dM$). The center support Δ_k^c of k -th RF was selected as a round area in the center of the field, its size was determined from the given ratio $\tau = \sigma_c^k / \sigma^k$ of the areas of the center and the RF (i.e. the size of the cent in pixels was $r = \sqrt{\tau/\pi} d$). The antagonistic environment was chosen as the addition of the center to the entire field $\Delta_k^s = \Delta_k \setminus \Delta_k^c$. The schematic image surface Ω partition (mosaic) by RF supports in numerical procedure implementation is presented in Figure 3.

Figures 4 shows the extracted from images contrast \tilde{n}_k^c (sharp changes in the reflection coefficient) of those RFs, where $\tilde{n}_k^c / \sigma_c^k \neq \tilde{n}_k^s / \sigma_s^k \neq (n_k + 1) / \sigma^k$ and their smoothed versions ($n_k + 1$) (slow changes in the illumination) of those RFs, where $\tilde{n}_k^c / \sigma_c^k = \tilde{n}_k^s / \sigma_s^k = (n_k + 1) / \sigma^k$ ($\tau = 0.2$, $d = 20$).

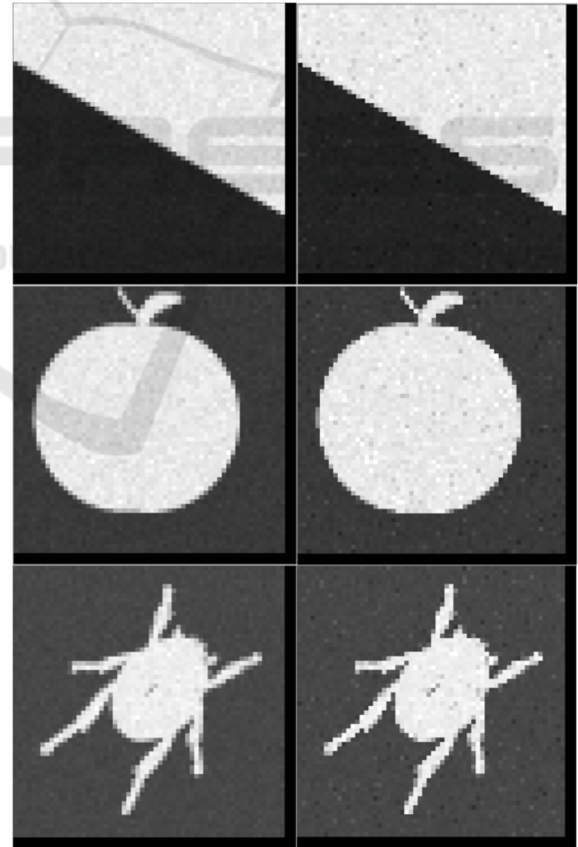


Figure 5: The comparison of smoothed and synthesised by RF shrinkage versions of Figure 1 images. Left column – smoothed version ($n_k + 1$), right column – synthesised version (\tilde{n}_k^c), see (32).

Figures 5 shows the comparison of smoothed versions ($n_k + 1$) (slow changes in the illumination + smoothed reflection coefficient) of all RFs, and their synthesised by RF shrinkage versions \tilde{n}_k^c (slow changes in the illumination + sharpened changes reflection coefficient) ($\tau = 0.2$, $d = 20$).

5 CONCLUSIONS

The approach proposed in the article, based on a low-count image RF shrinking, turned out to be very promising as it offers new possibilities for synthesis of real algorithms for nonlinear image reconstruction. A special representation of images (sampling representations) developed for these purposes made it possible, on the one hand, to avoid problems associated with the size of raster (bitmap) representations of images, and, on the other hand, opened wide opportunities for adapting machine learning methods.

A feature of the proposed approach is the concept of receptive fields. It provides both good image quality for human perception and effectively solves the problems associated with a huge number of mixture components (4) in the algorithmic implementation of the reconstruction problem.

We note here that the proposed approach has a natural extension to the area of parameter compression methods. As it turned out recently, it has numerous, non-trivial connections with such areas of machine learning as anisotropic diffusion methods, wavelet approaches and variational methods, which proved to be the best tools in the field of convolutional neural networks (Alt, 2020).

REFERENCES

- Aykroyd, R. G. (2015). Statistical image reconstruction. In *Industrial Tomography*, P. 401–427. Elsevier Ltd. DOI: 10.1016/B978-1-78242-118-4.00015-0.
- Caucci, L., Barrett, H. H. (2012). Objective assessment of image quality. V. Photon-counting detectors and list-mode data. In *Journal of the Optical Society of America. A, Optics, image science, and vision*, V. 29(6), P. 1003–1016. DOI:10.1364/JOSAA.29.001003
- Dougherty, G. (2009). *Digital Image Processing for Medical Applications*. Springer Science Business Media. NY. DOI: 10.1007/978-1-4419-9779-1.
- Oulhaj, H., Amine, A., Rziza, M., Aboutajdine, D. (2012). Noise Reduction in Medical Images – comparison of noise removal algorithms. In 2012 Intern. Conference on Multimedia Computing and Systems, P. 344–349. DOI:10.1109/icmcs.2012.6320218.
- Tomasi, C., Manduchi, R. (1998). Bilateral filtering for grey and colour images. In *Sixth International Conference on Computer Vision*. 98CH36271.IEEE, P. 839–846. DOI: 10.1109/ICCV.1998.710815.
- Perona, P., Malik, J. (1990). Scale-space and edge detection using Anisotropic Diffusion. In *IEEE Trans on Pattern Analysis and Machine Intelligence*, V. 12, P. 629–639.
- Rudin, L. I., Osher, S., Fatemi, E. (1992). Nonlinear total variation based noise removal algorithms. In *Physica. D*, V. 60(1), P. 259–268. DOI: 10.1016/0167-2789(92)90242-F.
- Weaver, J. B., Xu, Y., Healy Jr, D. M., Cromwell, L. D. (1991). Filtering noise from images with wavelet transforms. In *Magnetic Resonance in Medicine*, V. 21(2), P. 288–295. DOI: 10.1002/mrm.1910210213.
- Alt, T., Weickert, J., Peter, P. (2020). Translating Diffusion, Wavelets, and Regularisation into Residual Networks. // *arXiv:2002.02753*. DOI:10.48550/arxiv.2002.02753
- Blau, Y., Michaeli, T. (2019) Rethinking Lossy Compression: The Rate-Distortion-Perception Trade-off. In *Proc. of the 36th International Conference on Machine Learning, PMLR 97*, P. 675–685. DOI: 10.48550/arXiv.1901.07821.
- Werner, J.S., Chalupa, L.M. (2014). *The new visual neurosciences*. The MIT Press, Cambridge, Massachusetts.
- Schiller, P.H., Tehovnik, E.J. (2015). *Vision and the Visual System*. Oxford University Press, Oxford. DOI: 10.1093/acprof:oso/9780199936533.001.0001.
- Land, E.H., McCann, J. J. (1971) Lightness and retinex theory. In *Journal of the Optical Society of America*, V. 61(1), P. 1–11, 1971, DOI: 10.1364/JOSA.61.000001.
- Jobson, D. J., Rahman, Z., Woodell, G. A. (1997). Properties and performance of a center/surround retinex. // *In IEEE Transactions on Image Processing*, V. 6(3), P. 451–462. DOI: 10.1109/83.557356.
- Hai, J., Hao, Y., Zou, F., Lin, F., Han, S. (2023). Advanced RetinexNet: A fully convolutional network for low-light image enhancement. In *Signal Processing. Image Communication*, V.112, 116916. DOI: 10.1016/j.image.2022.116916.
- Antsiperov, V., Kershner, V. (2023). Retinotopic Image Encoding by Samples of Counts. In *M. De Marsico et al. (Eds.): ICPRAM 2021/2022, LNCS 13822*, P. 1–24, Springer Nature, Switzerland AG, DOI: 10.1007/978-3-031-24538-1_3.
- Antsiperov, V. (2021). Maximum Similarity Method for Image Mining. In *ICPR 2021, Part V. Lecture Notes in Computer Science*, V 12665, P. 301–313. Springer, Cham. DOI: 10.1007/978-3-030-68821-9_28.
- Fossum, E. (2020). The invention of CMOS image sensors: a camera in every pocket. In *2020 Pan Pacific Microel. Symp.*, P. 1–6. DOI: 10.23919/PanPacific.48324.2020.9059308.
- Streit, R. L. (2010). *Poisson Point Processes Imaging, Tracking, and Sensing*. Springer US: Imprint: Springer. DOI: 10.1007/978-1-4419-6923-1.
- Wilks, S. S. (1962). *Mathematical statistics*. John Wiley & Sons, Inc., Hoboken.

- Latecki, L. J., Lakamper, R., Eckhardt, T. (2000). Shape descriptors for non-rigid shapes with a single closed contour. In *Proceedings IEEE Conference on Computer Vision and Pattern Recognition. CVPR 2000 (Cat. No. PR00662)*, V.1, P. 424–429. DOI: 10.1109/CVPR.2000.855850.
- Robert, C.P., Casella, G. (2004) *Monte Carlo Statistical Methods*, 2nd ed. Springer-Verlag, New York. DOI: 10.1007/978-1-4757-4145-2.
- Milanfar, P. (2013). A Tour of Modern Image Filtering: New Insights and Methods, Both Practical and Theoretical. In *IEEE signal processing magazine*, V. 30(1), P. 106–128. DOI: 10.1109/MSP.2011.2179329.
- Hubel D.H., Wiesel, T.N. (2004). *Brain and Visual Perception: The Story of a 25-year Collaboration*. New York: Oxford University Press, 2004.
- Cho, M.W., Choi, M.Y. (2014). A model for the receptive field of retinal ganglion cells. In *Neural Networks*, V. 49, P.51–58. DOI: 10.1016/j.neunet.2013.09.005.
- Gauthier, J.L., Field, G.D., et al. (2009). Receptive fields in primate retina are coordinated to sample visual space more uniformly. *PLoS Biol.* V. 7(4), P. e1000063. DOI: 10.1371/journal.pbio.1000063.
- Field, G.D., Gauthier, J.L., et al. (2010). Functional connectivity in the retina at the resolution of photoreceptors. *Nature*, V. 467(7316), P. 673–677. DOI: 10.1038/nature09424.
- Donoho, D. L., Johnstone, J. M. (1994) Ideal spatial adaptation by wavelet shrinkage. In *Biometrika*, V. 81(3), P. 425–455. DOI: 10.1093/biomet/81.3.425.
- Mallat, S. G. (1989). A theory for multiresolution signal decomposition: the wavelet representation. In *IEEE Transactions on Pattern Analysis and Machine Intelligence*, V. 11(7), P. 674–693. DOI: 10.1109/34.192463.
- Sujith, V., Karthik, B. (2022). Removal of noise in Poisson image based on minimum risk wavelet shrinkage operator. *AIP Conference Proceedings*, V. 2426(1). DOI: 10.1063/5.0111528.
- Chipman, H.A., Kolaczyk, E.D., McCulloch, R.E. (1997). Adaptive Bayesian Wavelet Shrinkage. In *Journal of the American Statistical Association*, V. 92(440), P. 1413–1421. DOI: 10.1080/01621459.1997. 10473662.